JUSTC

Article

http://justc.ustc.edu.cn

Received: November 03, 2022; Accepted: January 16, 2023

# Observation of MLT region winds and tides by the USTC Mengcheng meteor radar

Wen Yi[1,2], Xianghui Xue[1,2,3,4,5] ✉, Jie Zeng[1,2], Jianyuan Wang[1,2], Baozhu Zhou[1,2], Hailun Ye[1,2], Tingdi Chen[1,2], and Xiankang Dou[1]

[1]*CAS Key Laboratory of Geospace Environment, School of Earth and Space Sciences, University of Science and Technology of China, Hefei 230026, China;*
[2]*Anhui Mengcheng Geophysics National Observation and Research Station, University of Science and Technology of China, Hefei 230026, China;*
[3]*CAS Center for Excellence in Comparative Planetology, Hefei 230026, China;*
[4]*Deep Space Exploration Laboratory, Hefei 230026, China;*
[5]*Collaborative Innovation Center of Astronautical Science and Technology, Hefei 230026, China*

✉Correspondence: Xianghui Xue, E-mail: xuexh@ustc.edu.cn


## Graphical abstract

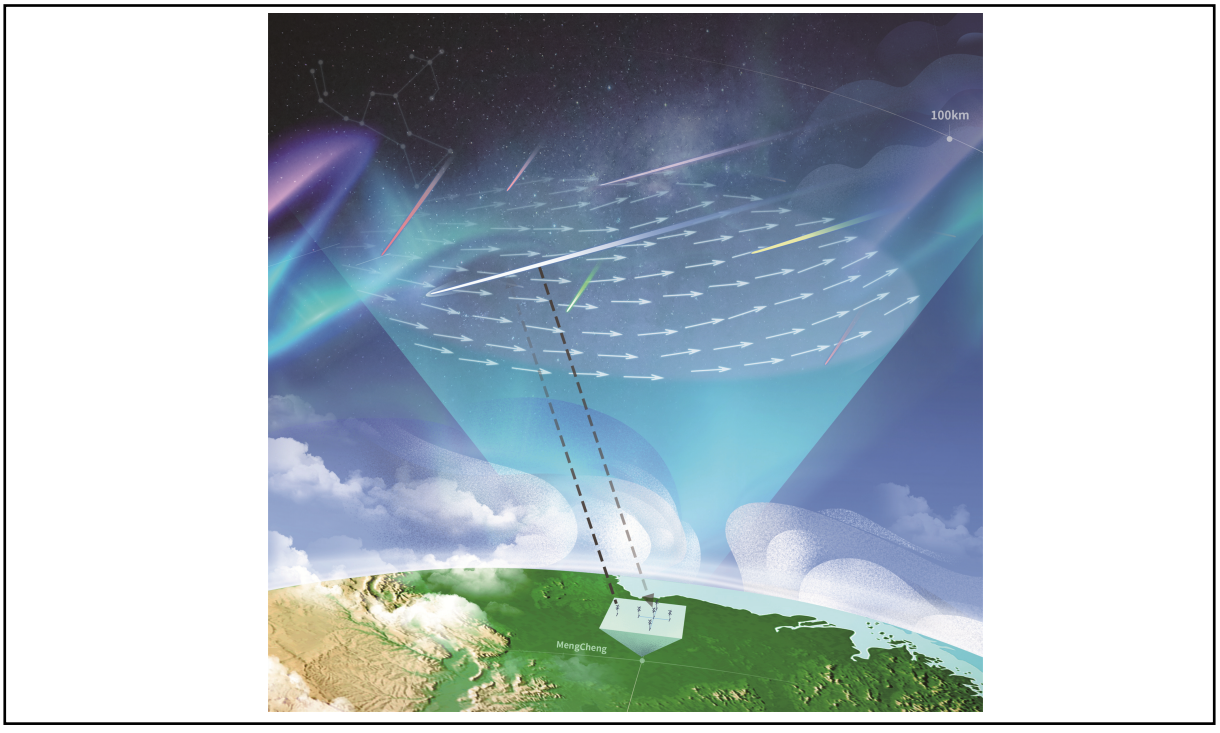


*Schematic diagram of a backward scatter geometry for the Mengcheng meteor radar.*

## Public summary

- More than 8 years of observation of mesospheric horizontal winds are presented in this study.
- Seasonal variations of mesospheric diurnal and semidiurnal tides at lower midlatitudes are obtained by the Mengcheng meteor radar.
- An intercomparison between the mesospheric measurements and NAVGEM-HA analysis results is presented.

**Citation:** Yi W, Xue X H, Zeng J, et al. Observation of MLT region winds and tides by the USTC Mengcheng meteor radar. *JUSTC*, **2023**, 53(5): 0501. DOI: 10.52396/JUSTC-2022-0158

JUSTC

Article

http://justc.ustc.edu.cn

Received: November 03, 2022; Accepted: January 16, 2023

# Observation of MLT region winds and tides by the USTC Mengcheng meteor radar

Wen Yi[1,2], Xianghui Xue[1,2,3,4,5] ✉, Jie Zeng[1,2], Jianyuan Wang[1,2], Baozhu Zhou[1,2], Hailun Ye[1,2], Tingdi Chen[1,2], and Xiankang Dou[1]

[1]*CAS Key Laboratory of Geospace Environment, School of Earth and Space Sciences, University of Science and Technology of China, Hefei 230026, China;*
[2]*Anhui Mengcheng Geophysics National Observation and Research Station, University of Science and Technology of China, Hefei 230026, China;*
[3]*CAS Center for Excellence in Comparative Planetology, Hefei 230026, China;*
[4]*Deep Space Exploration Laboratory, Hefei 230026, China;*
[5]*Collaborative Innovation Center of Astronautical Science and Technology, Hefei 230026, China*

✉Correspondence: Xianghui Xue, E-mail: xuexh@ustc.edu.cn


Cite This: *JUSTC*, **2023**, 53(5): 0501 (12pp)  Read Online

**Abstract:** The atmospheric winds and waves in the mesosphere and lower thermosphere (MLT) region are essential for studying the dynamics and climate in the middle and upper atmosphere. The University of Science and Technology of China (USTC) meteor radar located at Mengcheng (33.36°N, 116.49°E) has been operating continuously since April 2014. More than 8 years of observation of mesospheric horizontal winds and tides are presented in this study. In addition, we present an intercomparison among the meteor radar observations and the Navy Global Environmental Model-High Altitude (NAVGEM-HA) analysis results. The meteor number at northern lower midlatitudes suffers from diurnal variations in meteor occurrence, with a high count rate in the local morning and a low rate during local afternoon-to-midnight. The meteor count rates show a clear annual variation, with a maximum in September–October and a minimum in February. The horizontal wind in the MLT region has dominant annual variations at lower midlatitudes, with the eastward wind during summer and the westward wind during winter above 84 km, and the eastward wind during winter and the westward wind during spring below 84 km. The meridional wind is northward during winter and southward during summer. The diurnal amplitude is dominant, followed by the semidiurnal tides at lower midlatitudes. The zonal and meridional diurnal tides show enhancements during spring (March) with amplitudes that can reach up to 40 m/s and 30 m/s and during autumn (September) with amplitudes that can reach up to 30 m/s and 25 m/s, respectively. The seasonal variations in diurnal tidal amplitude basically show characteristics that are strong during the equinox and weak during the solstice. The zonal and meridional semidiurnal tides are maximized during spring (April) and autumn (September) above 90 km.

**Keywords:** mesosphere and lower thermosphere region; meteor radar; mesopause; horizontal wind; tides

**CLC number:** P407.2; P412.16; P412.22  **Document code:** A

## 1 Introduction

The mesosphere and lower thermosphere (MLT) are important connecting regions that couple the lower and upper atmosphere through a variety of atmospheric waves, such as gravity waves, tides and planetary waves[1, 2]. Observation of these atmospheric dynamic processes is very important for understanding the coupling between atmospheric layers. The upward propagation of atmospheric waves originating from the lower atmosphere into the MLT region drives the meridional circulation, resulting in upwelling and adiabatic cooling in the summer polar mesopause region.

In recent decades, significant development of ground-based techniques, such as radars and LIDARs, have permitted observations of MLT dynamics at different spatial and temporal scales, as well as their long-term climatology from the equator to the poles. In particular, meteor radar has become the most widely used instrument to routinely observe MLT winds among ground-based techniques because it has the advantages of being low cost, easy to install, and operate automatically and continuously under all weather conditions[3, 4]. Meteor radar operates both day and night under all kinds of weather and geographical conditions and provides good long-term observations; consequently, meteor radar is a powerful technique for studying the dynamics and climate of the mesopause region, including the wind fields[5–7], tidal waves[8, 9], planetary waves[10–12] and temperatures[13–17]. In addition to acquiring wind and temperature measurements, meteor radar has also been applied in recent years to estimate the atmospheric density in the mesopause region[18, 19].

In addition to ground radar techniques, atmospheric models have also been developed to predict MLT winds, temperatures and densities. For example, empirical models are based on synthesizing datasets from ground-based sounding rockets


DOI: 10.52396/JUSTC-2022-0158
*JUSTC*, **2023**, 53(5): 0501

and satellite measurements, such as the COSPAR International Reference Atmosphere CIRA-86[20], the Mass Spectrometer Incoherent Scatter (NRLMSISE-00) model[21] and the Horizontal Wind Model[22]. In general, the HWM model captures the seasonal variations in the MLT wind well and has better performance in the zonal component than in the meridional component[5, 23]. The mesospheric densities obtained by the MSIS model exhibit obvious differences from the meteor radar observations because the empirical MSIS based on observations were acquired over a decade ago; in particular, mesospheric density data were quite scarce at that time[19]. In addition, several general circulation models (GCMs) have been developed to assess not only short-term atmospheric wave variabilities but also climatological variations and long-term changes in the MLT region. For example, the Whole Atmosphere Community Climate Model Extension-Specified Dynamics (WACCM-X(SD)), the Ground-to-Topside Model of Atmosphere and Ionosphere for Aeronomy (GAIA), and the Upper Atmosphere ICOsahedral Nonhydrostatic (UA-ICON) model are based on GCMs. The WACCM model appears to capture the seasonal and latitudinal variations in the zonal wind component well, whereas the meridional wind exhibits differences from the meteor radar observations. The mesospheric tides obtained by the free-running UA-ICON show better agreement with the meteor radar observations compared to the WACCM results. The GAIA winds show reasonable agreement with the meteor radar wind measurements[6, 7]. The Navy Global Environmental Model-High Altitude (NAVGEM-HA) is a high-altitude meteorological analysis system for numerical weather prediction (NWP), which assimilates satellite-based observations of temperature, ozone and water vapour in the stratosphere, mesosphere and lower thermosphere[24]. Stober et al.[25] compared the NAVGEM-HA wind with three meteor radars located at the northern high (Andenes (69°N, 11°E) in Norway) and middle latitudes (Juliusruh (54.3°N, 13°E) and Tavistock (43.2°N, 80.7°W)) and indicated good consistency in seasonal variations in MLT winds between them. Thus, the Mengcheng meteor radar measurements at lower midlatitudes can be used to examine the performance of NAVGEM-HA analyses data of the MLT region.

The goal of this study is to introduce measurements in the MLT region observed by the University of Science and Technology of China (USTC) meteor radar located at Mengcheng (33.36°N, 116.49°E). In addition, we present an intercomparison among the meteor radar and NAVGEM-HA analysis results. The rest of the paper is organized as follows. In Section 2, we introduce the experimental instruments and their datasets. Then, in Sections 3 and 4, we present the seasonal variations in mesospheric wind and their tides observed by the Mengcheng meteor radar, respectively. Finally, we summarize our results.

## 2 Instruments and datasets

### 2.1 The Mengcheng meteor radar

The Mengcheng all-sky interferometric meteor radar (MCMR) was installed at the Mengcheng station (33.36°N, 116.49°E) in Anhui Province, China. The MCMR has been operating by the University of Science and Technology of China (USTC) since April 2014. The MCMR is an Atmospheric Radar Systems (ATRAD) meteor detection radar and is essentially the same as that described by Holdsworth et al.[4] Fig. 1 shows a schematic diagram of a backscatter geometry for an all-sky meteor radar. Table 1 summarizes the system parameters. The MCMR transmits a coherent pulsed radio signal at a frequency of 38.9 MHz corresponding to a wavelength of $\lambda = 7.71$ m and a peak power of 20 kW. The MCMR employs a 4-bit code and a pulse repetition frequency of 430 Hz with four sample integrations. A single crossed and folded dipole is used for transmission. Five two-element Yagi antennas composing a cross '+' shape arrangement positioned on two orthogonal baselines[26] are used for reception, also displayed in Fig. 1. On each baseline, the outer antennas are separated from the center by $2\lambda$ and $2.5\lambda$. The $2\lambda$ and $2.5\lambda$ space arrangements can reduce the mutual antenna coupling. The phase differences between antenna pairs are combined to produce a virtual half-wavelength baseline to unambiguously determine the azimuth and elevation of the meteor echoes and provide excellent angular resolution for position determination[26]. Fig. 1 also shows the horizontal projection of 17191 meteor echoes observed by the MCMR on October 16, 2021. The backscattered echoes are observed in an approximately 300 km radius and are mainly distributed 50–150 km from the MCMR.

In this study, hourly horizontal zonal and meridional wind measurements with 2 km height resolution observed by the MCMR are used to investigate the seasonal variations in horizontal wind and to extract the mesospheric tides in the MLT regions at northern lower midlatitudes. Reid et al.[27] and Zeng et al.[28] carried out joint measurement campaigns involving two meteor radars located at Davis Station in Antarctica and at Kunming Station at low latitudes, respectively, and summarized the performance of wind measurements observed by meteor radar and provided a precise estimation of wind uncertainties.

Fig. 2a shows the height-local time distribution of meteor echoes observed by the MCMR from October 16 to October 20, 2021. The meteor count rate observed by the MCMR shows a clear diurnal variation, with a high count rate in the local morning (i.e., 0200–1000 LT) and a low count rate during local afternoon-to-midnight (i.e., 1400–2400 LT). In

**Table 1.** Main operation parameters of the Mengcheng meteor radar.

| | |
|---|---|
| Frequency | 38.9 MHz |
| Peak power | 20 kW |
| Pulse repetition frequency | 430 Hz |
| Transmission mode | Circular |
| Coherent integrations | 4 |
| Range resolution | 1.8 km |
| Pulse type | Gaussian |
| Pulse width | 24 μs |
| Duty cycle | 15% |
| Detection range | 70–110 km |


DOI: 10.52396/JUSTC-2022-0158
*JUSTC*, **2023**, 53(5): 0501

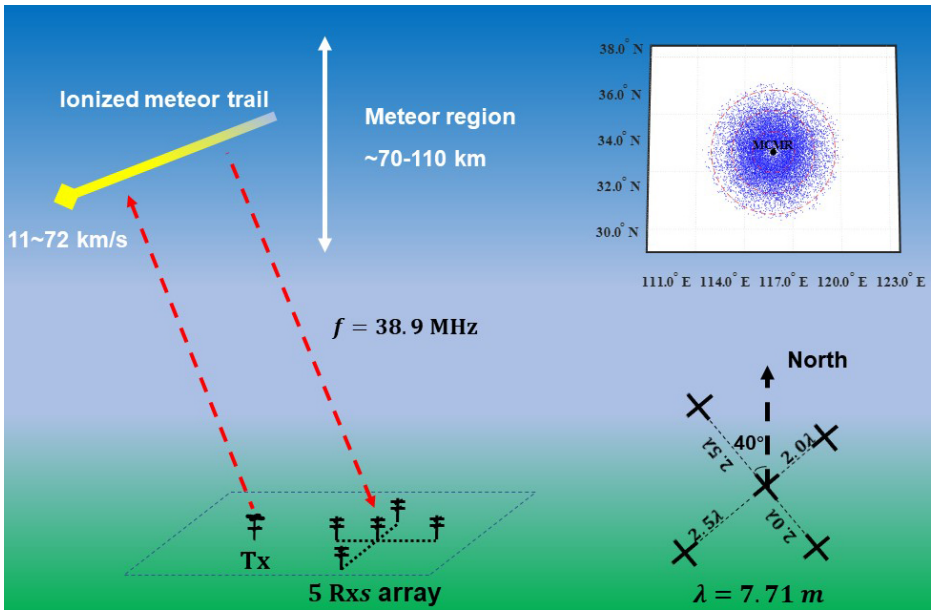


**Fig. 1.** Schematic diagram of a backward scatter geometry for the Mengcheng meteor radar. The left bottom shows the five element Yagi antennas using a cross '+' shape arrangement used for reception. The left upper panel shows the horizontal projection of 17191 meteor detections (blue dots) observed by the MCMR on October 16, 2021. The red dot represents the location of MCMR. The red circles represent distances of 100 km, 200 km and 300 km to the MCMR.

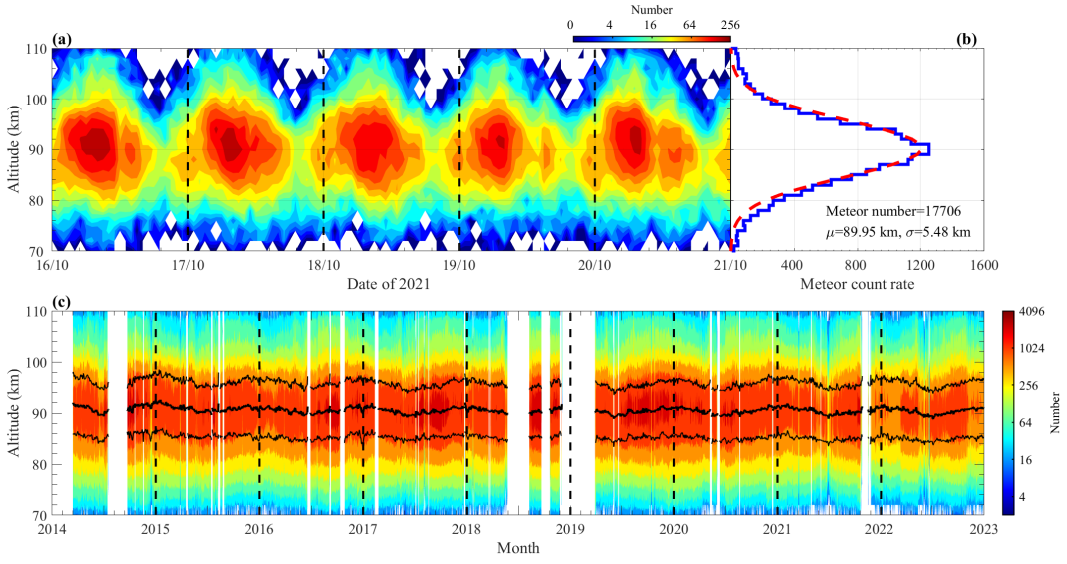


**Fig. 2.** (a) Diurnal (local time) variation in meteor number observed by MCMR from October 16 to October 20 in 2021. (b) Histogram of the meteor height distribution observed by the MCMR on October 16, 2021. The fitted Gaussian curves are used to estimate the peak height ($\mu$) and standard deviation ($\sigma$) of the meteor height distribution. (c) The height-time section of meteor counts with a grid of [2 km, 1 day] observed by the MCMR. The black solid lines represent the peak height ($\mu$) and upper ($\mu+\sigma$) and lower ($\mu-\sigma$) widths of the meteor height distribution.

Fig. 2b, the meteor echoes are distributed at altitudes of 70–110 km. As shown by the red fitting curve, the height distributions of meteor echoes are well approximated by a fitted Gaussian curve. Fig. 2c shows the time-height distribution of meteor echoes observed by the MCMR. Measurements obtained by the KMMR from April 2014 to December 2022 are used in this study. Although there are some data gaps due to site maintenance, the MCMR data still have good continuity for investigating the atmospheric dynamics and climatology in the MLT region at lower midlatitudes.

Fig. 3a shows the daily meteor number observed by the MCMR. The MCMR typically detects approximately 6000–20000 underdense meteor echoes per day, of which approximately 200–1600 meteor echoes occur per hour. The seasonal variations in the meteor count rates observed by the MCMR (at northern lower midlatitudes) show a clear annual variation, with a maximum in September–October and a minimum in February. These results are similar to the observations at northern middle and high latitudes made by Singer et al.[29] Yi et al.[18] reported that the meteor count rate at northern low latitudes shows annual variation, with a maximum in July and a minimum in late March. Interestingly, meteor


DOI: 10.52396/JUSTC-2022-0158
*JUSTC*, **2023**, 53(5): 0501

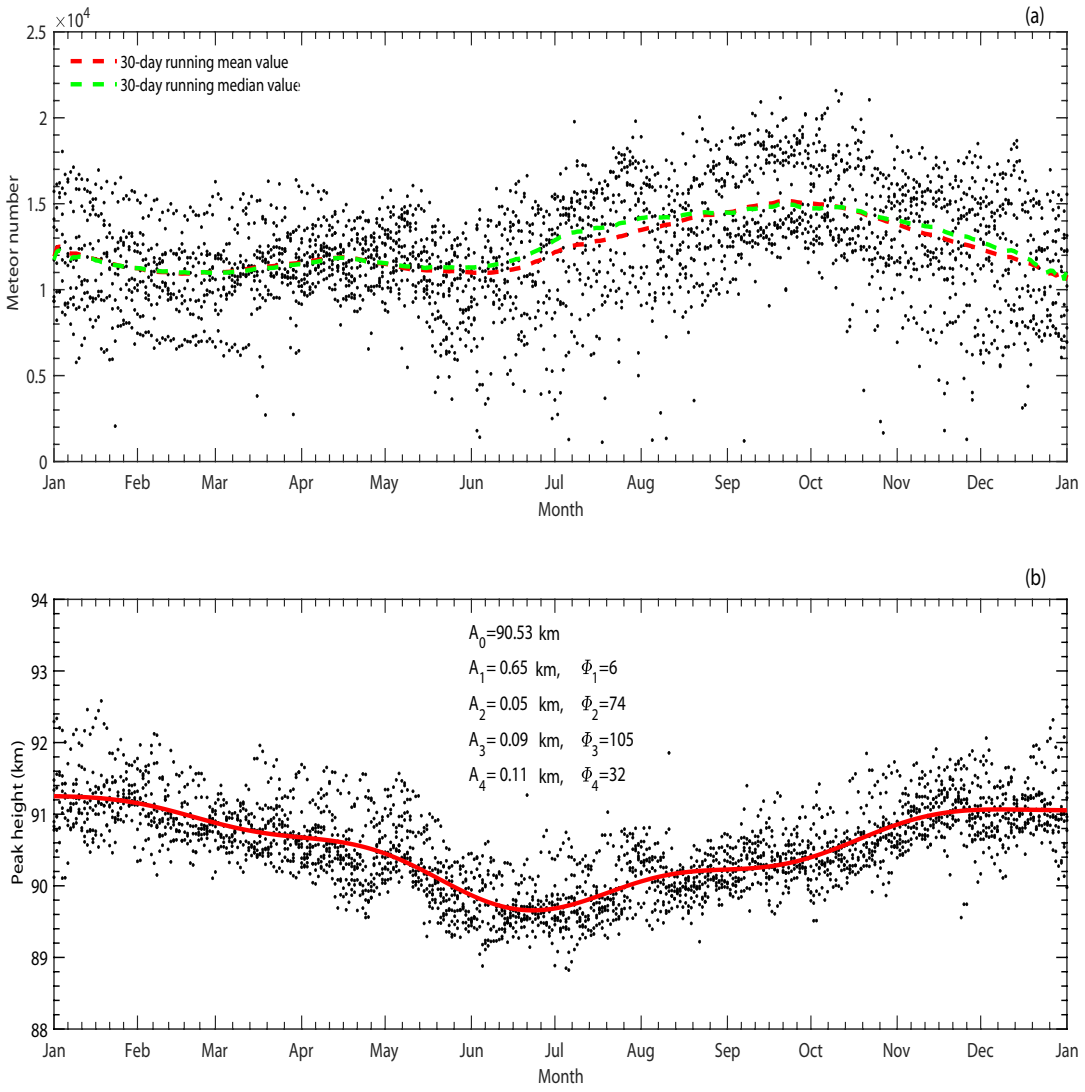


**Fig. 3.** Scatterplot of the composite (a) meteor count rate and (b) peak height of the meteor detection distribution as a function of the day of the year. The red and green dashed lines represent the 30-day running mean and median values. The red line represents the harmonic fits consisting of annual, semiannual, terannual, and quarterly (periods of 365, 182.5, 121, 91 days) components for the composited peak height. ($A_1$, $A_2$, $A_3$, $A_4$) and ($\Phi_1$, $\Phi_2$, $\Phi_3$, $\Phi_4$) represent the amplitudes and phases of the annual, semiannual, terannual, and quarterly components, respectively.

count rates observed at southern high latitudes by Janches et al.[30] and Reid et al.[31] showed a maximum in January and a minimum in June. Their results reveal a clear spatial asymmetry and different seasonal variations in meteoroid inputs in the global distribution, which is important for understanding the deposition of meteoric material in the MLT region.

Fig. 3b shows the composite analysis of the peak height of the meteor height distribution observed by the MCMR. The MCMR at northern lower midlatitudes mainly shows annual variation, with a maximum in winter and a minimum in summer. A harmonic fit of annual, semiannual, terannual, and quadrennial components for peak heights shows a maximum in midwinter (i.e., January) of approximately 91 km and a minimum in midsummer (i.e., July) at approximately 88.5 km. The peak height after removing the meteor velocity effects shows a strong linear correlation with the mesospheric density, which indicates that the peak height can also be used as a proxy for the neutral atmospheric density[18].

## 2.2 NAVGEM-HA meteorological analysis data

NAVGEM-HA is an extension of the Navy operational weather forecast system up to 6 × $10^{-5}$ hPa (~116 km altitude), and the vertical spacing is ~2 km in the stratosphere and mesosphere[24, 32]. The top levels of the system above ~100 km altitude are specified with strong diffusion to reduce the wave reflection. Thus, only analysis results below ~100 km are valid. NAVGEM-HA has provided a global description of atmospheric wind, temperature and composition from the surface to ~100 km. The system assimilates temperature, ozone mixing ratio, and water vapour mixing ratio profiles observed by the Microwave Limb Sounder (MLS) onboard the Aura satellite, temperature profiles observed by the Sounding of the Atmosphere Using Broadband Emission Radiometry (SABER) instrument onboard the Thermosphere, Ionosphere, Mesosphere Energetics and Dynamics (TIMED) satellite, and microwave radiances from the Upper Atmosphere Sounding


DOI: 10.52396/JUSTC-2022-0158
*JUSTC*, **2023**, 53(5): 0501

(UAS) channels of the Special Sensor Microwave Imager/Sounder (SSMIS) onboard the Defense Meteorological Satellite Program (DMSP) F17 satellite. The assimilation is performed every 6 h, and by including the 3-hour forecast output of atmospheric variables, global wind fields are generated every 3 h on a 1° latitude × 1° longitude grid[24]. In this study, we extract the horizontal wind and tides using the NAVGEM-HA output from December 2009 to December 2010 over the MCMR to conduct an intercomparison between the NAVGEM-HA analysis data and meteor radar observations.

## 3 Seasonal variations in MLT winds observed by the Mengcheng meteor radar

Fig. 4a shows the 8-year monthly mean zonal wind between altitudes of 76 and 100 km. The mean zonal wind mainly shows an annual variation, with a strong eastward wind during summer with a maximum of approximately 50 m/s and a weak westward wind during winter with a maximum of approximately 10 m/s above 84 km. Below 84 km, the mean zonal wind shows an annual variation, with a strong eastward wind during winter and a weak westward wind during spring, with a maximum of approximately 20 m/s. Fig. 4b shows the monthly mean variation in meridional wind. The meridional wind mainly shows annual variation, with a strong northward wind during winter with a maximum of approximately 20 m/s and southward wind during summer with a maximum of approximately 15 m/s.

As shown in the Lomb-Scargle periodogram, the zonal and meridional winds show weak semiannual variations below 84 km and above 90 km, respectively. In general, at midlatitudes, the annual and semiannual variation amplitudes of the zonal wind are larger than those of the meridional wind; meanwhile, the annual variation is stronger than that of the semiannual variation. For the MCMR observations, the annual variation amplitudes in the zonal and meridional components clearly reach maxima of approximately 20 m/s and 10 m/s, respectively, while the amplitudes of the semiannual variations reach maxima of approximately 12 m/s and 10 m/s, respectively.

In addition, the Lomb-Scargle periodograms of zonal and meridional winds also exhibit weak periodicities of 120 and 90 d. A few studies have reported the evident signature of quasi-120-day and 90-day oscillations in MLT winds, tides, temperatures, ozone concentration[33–36] and OH intensity[37]. Although the mechanisms of the quasi 120-day and 90-day oscillations are still not certain, the origin source is generally believed to link the upper and lower atmosphere through the upward propagation of atmospheric waves. The plausible mechanism is the similar periodic modulation of the tropospheric excitation of the waves (probably associated with convection) and subsequent enhancement by ozone (stratosphere), causing the manifestation of the oscillation in the MLT[34–36].

Fig. 5 shows the composite of monthly mean zonal and meridional winds from 2014 to 2021 observed by the Mengcheng meteor radar (upper row) and the monthly mean SABER temperatures compared to the monthly mean zonal and meridional winds and temperature wind derived NAVGEM-HA during 2009. The zonal winds in Fig. 5a indicate a clear annual variation, with strong eastward winds in summer/winter above/below 84 km. The zonal wind shows a typical eastward wind in winter and reverses to a westward wind in spring. In addition, a vertical wind shear during winter and summer occurs near an altitude of 86 km. The zonal wind output by NAVGEM-HA in Fig. 5b shows similar behavior, but the magnitude of the winds is to some extent larger compared to the MCMR observations.

In Fig. 5c, the meridional winds are northward and up to 10 m/s during winter, and southward wind during summer up to 15 m/s. The meridional winds reverse from northward/

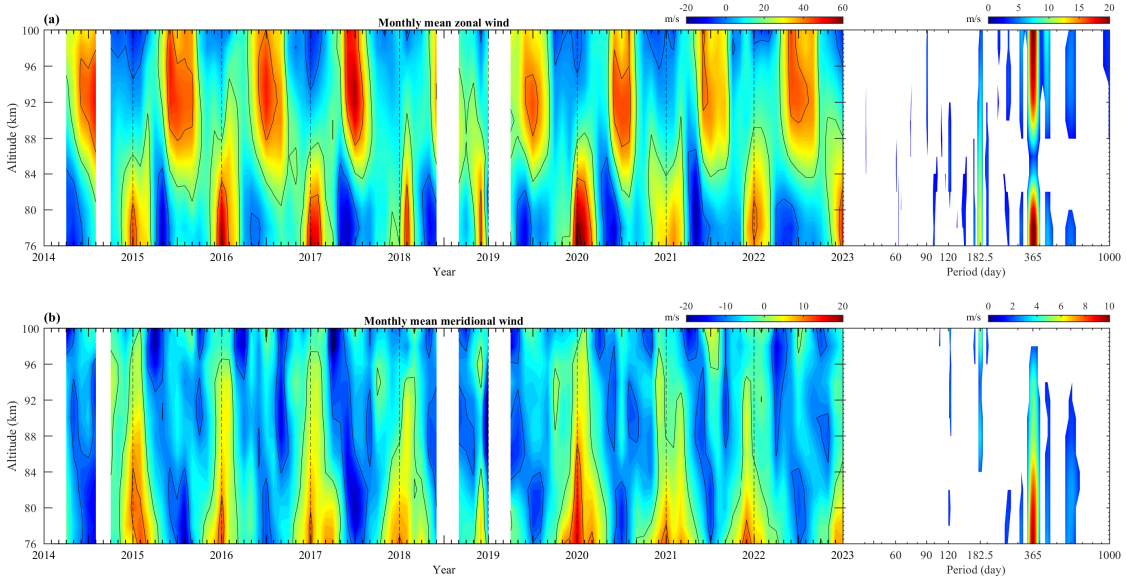


**Fig. 4.** (a) Monthly mean zonal (eastward is positive) and (b) meridional (northward is positive) winds from 2014 to 2022 observed by the MCMR between altitudes of 76 and 100 km. Contour plot of the Lomb-Scargle (LS) periodogram spectra corresponding to the daily mean zonal and meridional winds corresponding to the right column; the LS periodogram amplitudes are above the 95% confidence level.


DOI: 10.52396/JUSTC-2022-0158
*JUSTC*, **2023**, 53(5): 0501

southward to southward/northward near the spring/autumn equinox. The meridional wind output by the NAVGEM-HA in Fig. 5d shows similar seasonal variations to the MCMR observations, while there are still some differences between the NAVGEM-HA output and MCMR meridional winds above 92 km. For example, the NAVGEM-HA output shows a larger northward wind than the MCMR measurements. Fig. 5e shows monthly mean temperatures in the MLT region over the MCMR from the SABER measurements. The temperature obtained from SABER profiles (version 2.0) from 2014 to 2021 was selected from a 5°×20° grid centered on the meteor radar locations, and the satellite temperature observations taken on the same days as the meteor radar measurements were averaged for daily mean temperature. Remsberg et al.[38] suggested that the systematic error of the SABER temperature is no more than 2 K below a height of 70 km, while in the upper mesosphere to lower thermosphere region, the error increases with altitude from 1.8 K at 80 km to 6.7 K at 100 km. The SABER temperatures show the annual variation in MLT regions, including the cold summer mesopause, where the summer temperatures fall to below 170 K between altitudes of 80 and 90 km. In general, the seasonal variations in the NAVGEM-HA temperatures in Fig. 5f show good agreement with the SABER measurements, although we note that the NAVGEM-HA temperatures are warmer during summer and colder during winter. The NAVGEM-HA analysis data tend toward larger variations in temperature. These slightly larger temperature fluctuations in the NAVGEM-HA data may also explain the higher wind magnitudes relative to the MCMR observations[25].

## 4 Atmospheric tides in MLT wind observed by the Mengcheng meteor radar

In this section, we investigate the seasonal variation in the solar tides in the MLT wind observed by the MCMR. Fig. 6a and 6b show the Lomb-Scargle periodogram of zonal and meridional hourly winds at 90 km altitude. It is clear that the diurnal tides with a periodgram of 24 h dominate the MLT wind at lower midlatitudes, and the second strongest is the semidiurnal tides. The periodgrams of 8 and 6 h corresponding to the terdiurnal and quarterdiurnal tides can also be observed by the MCMR, but these amplitudes are much weaker than those of diurnal and semidiurnal tides. In addition, a periodogram peak is clearly visible near 12.42 h above the

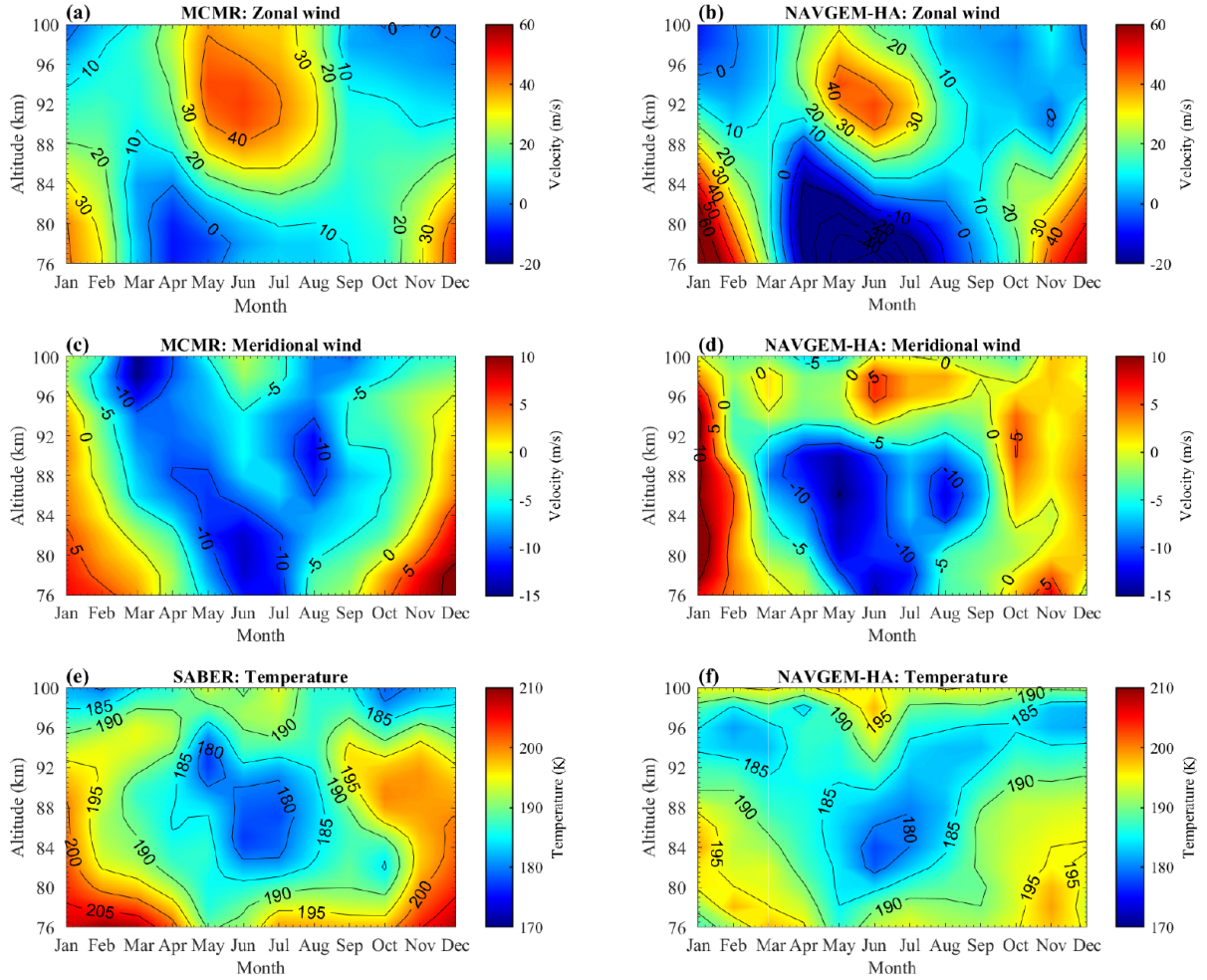


**Fig. 5.** Composite of monthly mean (a) zonal and (c) meridional winds from 2014 to 2022 observed by the Mengcheng meteor radar compared to the NAVGEM-HA derived monthly (b) zonal and (d) meridional winds. (e, f) Comparison of monthly mean SABER temperatures and NAVGEM-HA derived temperatures over the MCMR.


DOI: 10.52396/JUSTC-2022-0158
*JUSTC*, **2023**, 53(5): 0501

95% significance level, which likely corresponds to the semi-diurnal lunar tide. This suggests that the MCMR observations can be used to investigate the lunar tide and its climatology at middle latitudes[39]. Furthermore, some periods longer than 1 d at peaks near 2, 6, and 16 d are also found, which may correspond to known planetary wave periods[12, 40–43]. However, to confirm the modes of these planetary waves, a combination of ground-based and satellite measurements is still needed[42–44]. Therefore, the dominant dynamics of the large-scale zonal and meridional winds observed by the MCMR are diurnal and semidiurnal tides.

To directly examine the tidal dynamics from the MLT wind observed by the MCMR, we composite the hourly variation in mean zonal and meridional wind divided into four seasons. In Fig. 6, we also show examples of tidal structures during the spring and autumn equinoxes and the summer and winter solstices. In general, the vertical tidal structures all indicate the upward propagation of tides throughout the year. As shown in Fig. 6c–d and i–j, the composite zonal and meridional winds during the spring equinox and winter solstice show distinct vertical structures in the diurnal tides. In Fig. 6e–f and g–h, the zonal and meridional winds during the summer solstice and autumn equinox show the composite structures of diurnal and semidiurnal tides.

To better extract the tidal components observed by the MCMR, we calculate the amplitude and phase of tidal components. The tidal analysis involves harmonics fitted to the hourly mean zonal and meridional winds. The fitting function is given by

$$y(t) = \bar{y}(t) + \sum_{i=1}^{3} A_i \sin\left(\frac{2\pi i}{24} t + \phi_i\right), \tag{1}$$

where $y(t)$ is wind measurements, $\bar{y}(t)$ is the prevailing com-

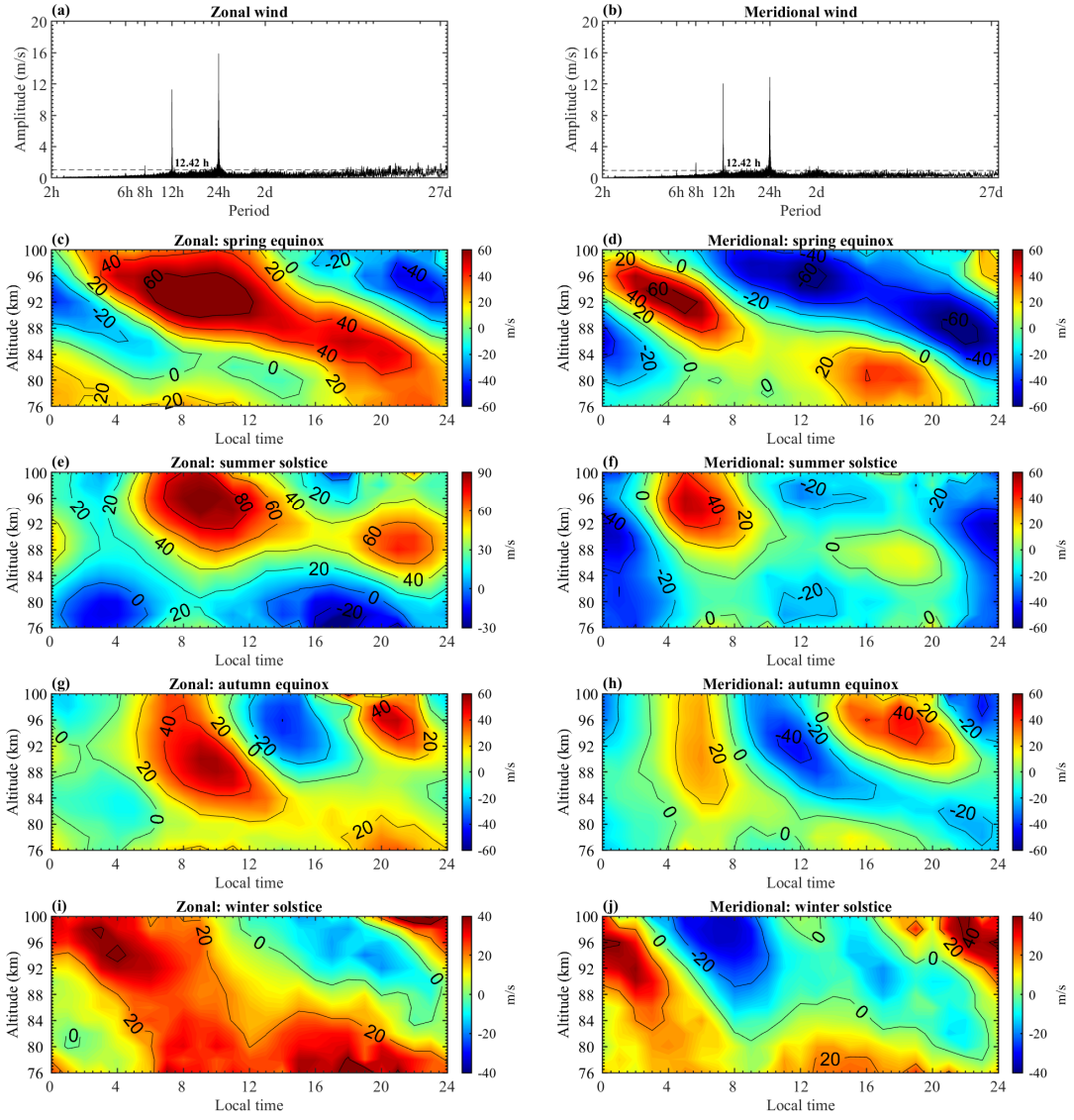


**Fig. 6.** Lomb-Scargle periodogram of the zonal (a) and meridional (b) hourly winds at 90 km altitude measured by the Mengcheng meteor radar for the period 2014 to 2022. Annotations show peaks corresponding to 24-, 12- and 8-hour solar tides, as well as the 12.42-hour lunar tide and quasi-2-day planetary waves. The dashed lines show the 95% confidence level. Hourly mean zonal (left column) and meridional (right column) wind composite for 21-day intervals centered on (second row) spring equinox, (third row) summer solstice, (fourth row) autumn equinox and (fifth row) winter solstice in 2016.


DOI: 10.52396/JUSTC-2022-0158
*JUSTC*, **2023**, 53(5): 0501

ponent, and $A_i$ and $\phi_i$ represent the amplitude and phase, respectively. The tidal components with periods of 24 h, 12 h and 8 h represent the diurnal, semidiurnal and terdiurnal tides, respectively.

Fig. 7 shows the monthly amplitudes and phases of the zonal and meridional diurnal tidal components averaged for the period from 2014 to 2022. Our results show that the diurnal amplitude is dominant at lower midlatitudes, especially during early spring (March), with amplitudes that can reach up to 40 m/s and 30 m/s in the zonal and meridional winds above 90 km, respectively. In addition, the diurnal amplitudes also show a second peak during autumn (September), basically following the characteristics of a strong peak during the equinox and a weak peak during the solstice[45]. The zonal component of the diurnal tide is consistently larger than that of the meridional diurnal tide. As shown in Fig. 7b, d, the NAVGEM-HA model only captures the zonal and meridional diurnal tidal enhancements during the spring (March) and autumn (September). However, these tidal enhancements appear at lower altitudes, with smaller amplitudes. Meanwhile, weak enhancements in diurnal tides during summer (June, July and August) were observed by the MCMR, which are not seen in the NAVGEM-HA model.

The zonal and meridional diurnal tidal phases observed by the MCMR at lower midlatitudes basically remain stable throughout the year. Both of the diurnal phases are indicative of upward propagating tides. The diurnal tidal vertical wavelengths during summer and winter are generally longer

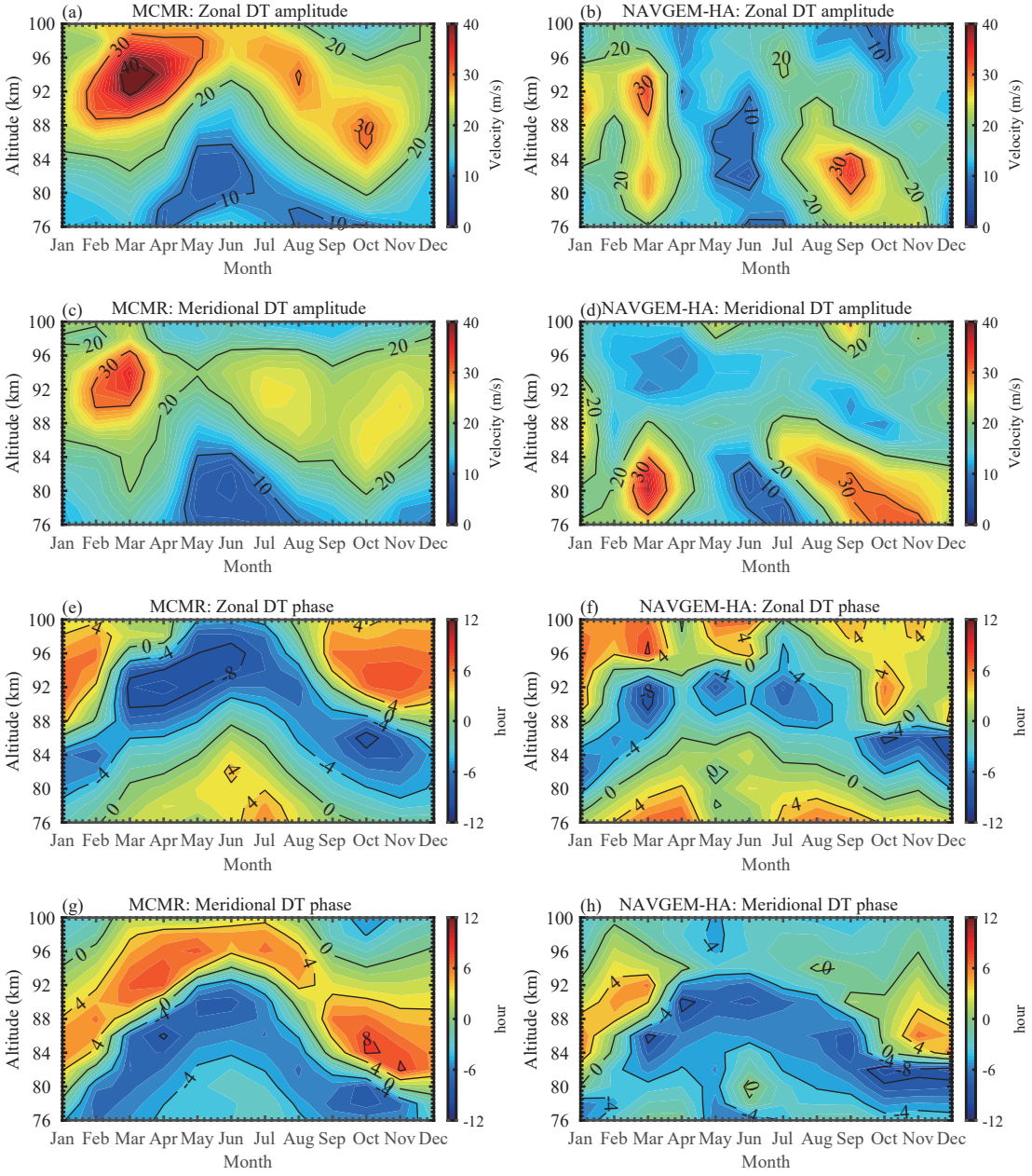


**Fig. 7.** Composite of zonal and meridional diurnal tidal (DT) amplitude (two upper rows) and phase (two lower rows) estimated by using the hourly wind measurements from 2014 to 2022 observed by the Mengcheng meteor radar (left column). The right column shows the zonal and meridional DT amplitude and phase estimated by the NAVGEM-HA results.


DOI: 10.52396/JUSTC-2022-0158
*JUSTC*, **2023**, 53(5): 0501

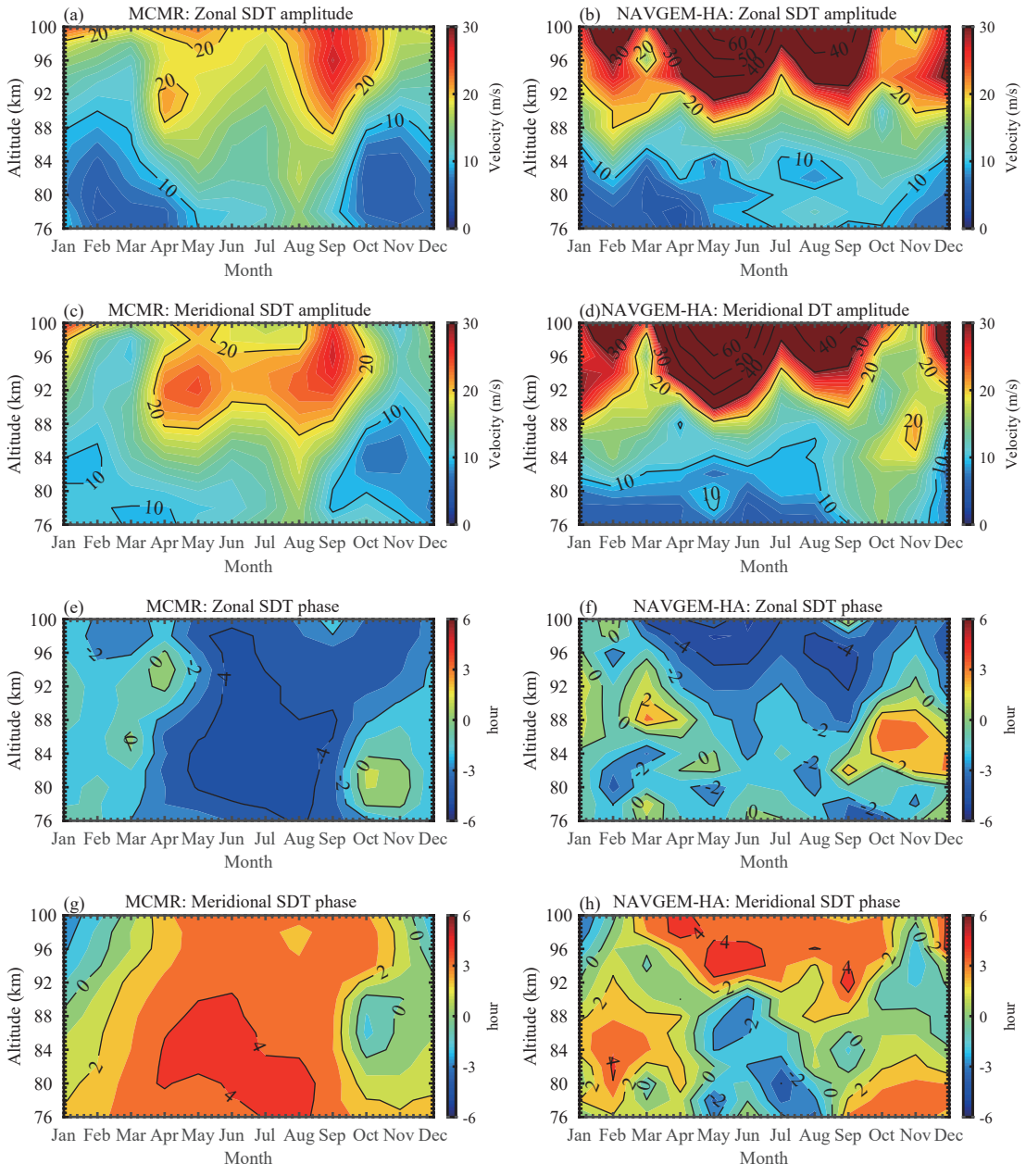


**Fig. 8.** Same as Fig. 7 but for semidiurnal tidal (SDT) amplitude and phase components.

than those during spring and autumn. There are approximately 8–10 h phase lags between the zonal and meridional components. It is encouraging to find that the NAVGEM-HA output shows good agreement with the MCMR observations. Diurnal tidal structures in the MLT region are extremely complex. Therefore, successfully modeling tidal structures requires an understanding of a wide range of atmospheric phenomena, including atmospheric radiation, chemistry, and dynamics. For example, Zhou et al.[7] compared the diurnal tides between the MCMR measurements and WACCM-SD output and indicated that the WACCM-SD generally fails to capture the seasonal behavior of the diurnal tides.

Fig. 8 shows the monthly semidiurnal tidal amplitudes and phases. In general, the semidiurnal tides are weaker than the diurnal tides at midlatitudes. The semidiurnal tides reach values up to 30 and 25 m/s in the zonal and meridional components, respectively. The semidiurnal tide is maximized during spring (April) and autumn (September) above 90 km. Similar to the diurnal tides, the zonal semidiurnal tides are stronger than the meridional semidiurnal tides. The zonal and meridional semidiurnal tides output by the NAVGEM-HA model show strong enhancements in a whole year with maxima during February, May, September and December and have larger amplitudes than the MCMR measurements. The model results can capture some similarities with the observations. For example, weak and strong semidiurnal tides appear during winter and summer below 90 km, respectively.

Fig. 8e, g shows the zonal and meridional semidiurnal tidal phases. The values of semidiurnal tidal phases generally decrease with increasing altitude, which indicates that the semidiurnal tide is again consistent with an upwardly propagating tide. Both the zonal and meridional semidiurnal


DOI: 10.52396/JUSTC-2022-0158
*JUSTC*, **2023**, 53(5): 0501

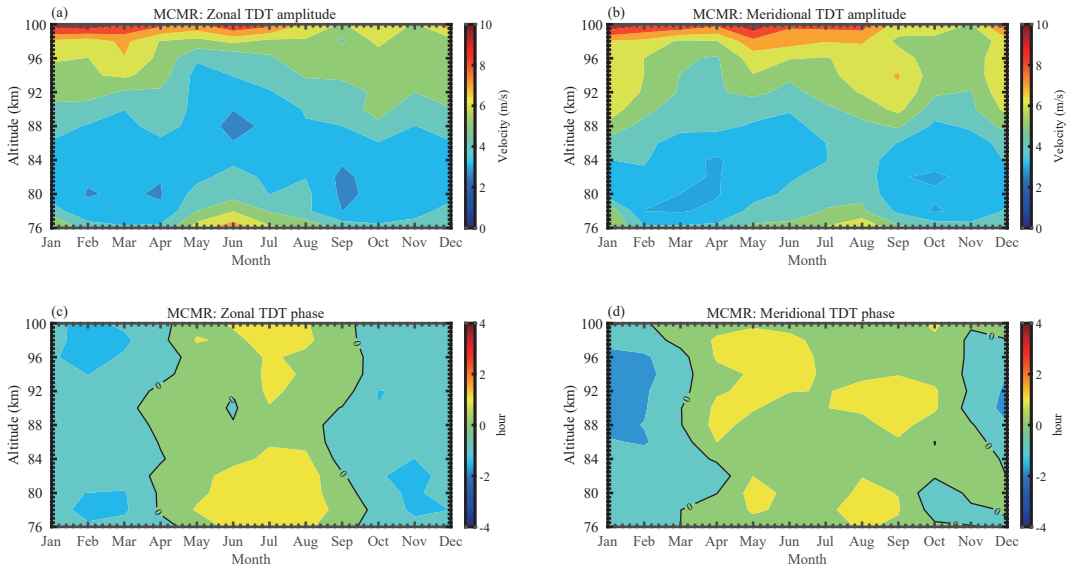


**Fig. 9.** Composite of zonal and meridional terdiurnal tidal (TDT) amplitude (upper row) and phase (lower row) estimated using the hourly wind measurements from 2014 to 2022 observed by the Mengcheng meteor radar.

tidal phases show quick phase changes during spring and autumn. There is an approximately 6-hour (half cycle) phase lag between the zonal and meridional components. The NAVGEM-HA semidiurnal tidal phase basically does not capture the seasonal characteristics compared to the observations.

As mentioned above, the NAVGEM-HA only provides the 3-hour time resolution of wind. This limits the estimation of the terdiurnal (8-hour) tidal component using the NAVGEM-HA data. Therefore, we present only the terdiurnal tide estimated by using the MCMR measurements. Fig. 9 shows the terdiurnal tide obtained from radar measured zonal and meridional tides. The zonal and meridional terdiurnal tides are relatively stable during the whole year and show enhancement above 92 km. However, the terdiurnal tide shows an enhancement during summer below 80 km. The phases of the zonal and meridional terdiurnal tides are basically 0000–0200 LT from April to October and 2200–0000 LT from November and March.

## 5 Conclusions

The Mengcheng meteor radar (33.36°N, 116.49°E) made near continuous measurements of winds in the mesosphere and lower thermosphere from March 2014 to present, which has good continuity for investigating the atmospheric dynamics and climatology in the MLT region at lower midlatitudes. Here, we presented more than 8 years of atmospheric horizontal winds and tides in the MLT region over Mengcheng and compared our measurements with the NAVGEM-HA analysis results. The main points we found are summarized as follows:

(Ⅰ) Approximately 6000–20000 underdense meteor echoes are observed per day by the Mengcheng meteor radar, which is sufficient for the estimation of hourly mean wind, daily temperature and density in the MLT region. The meteor number over Mengcheng at lower midlatitudes in the Northern Hemisphere suffers from diurnal variations in meteor occurrence, with a high count rate in the local morning (i.e., 0200–1000 LT) and a low count rate during the local afternoon-to-midnight (i.e., 1400–2400 LT). The meteor count rates observed by the MCMR show a clear annual variation, with a maximum in September–October and a minimum in February.

(Ⅱ) The horizontal wind in the MLT region has dominant annual variations at lower midlatitudes. The zonal wind shows the eastward wind during summer and the westward wind during winter above 84 km and shows the eastward wind during winter and the westward wind during spring below 84 km. The meridional wind is northward during winter and southward during summer below 90 km. The meridional winds reverse from northward/southward to southward/northward near the spring/autumn equinox.

(Ⅲ) The diurnal tide is dominant at lower midlatitudes, especially during early spring (March), with amplitudes that can reach up to 40 m/s and 30 m/s in the zonal and meridional winds above 90 km, respectively. In addition, the diurnal amplitudes also show a second peak during autumn (September), basically following the characteristics that are strong during the equinox and weak during the solstice.

(Ⅳ) Comparisons of the climatology of the atmospheric winds and tides in the MLT region among the Mengcheng meteor radar and the NAVGEM-HA analyses results. NAVGEM-HA effectively captures the seasonal variations in mesospheric winds. In addition, the NAVGEM-HA model roughly captures the prevailing annual variation in the diurnal tides but almost fails to capture the seasonal variations in the semidiurnal tides.

These results highlight the important contribution of MLT measurements made by the Mengcheng meteor radar, which can develop our understanding of the MLT winds and dynamics. A climatology of neutral temperatures and densities near the mesopause estimated using the ambipolar diffusion coefficient observed by the Mengcheng meteor radar will be reported in the following paper. These long-term continuous obser-


DOI: 10.52396/JUSTC-2022-0158
*JUSTC*, **2023**, 53(5): 0501

vations provide a wide range of potential to improve widely used atmospheric models. In addition to the now dominant all-sky monostatic (backscatter) meteor radar, research results will be reported in future that describe the first multi-static meteor radar system in China consisting of the Mengcheng meteor radar and a bistatic remote receiver located at Changfeng (31.98°N, 117.22°E) in Hefei city and present preliminary results of the derived two-dimensional wind fields in the MLT region over Central-Eastern China.

## Data availability

The Mengcheng meteor radar data presented in this study are available on request from the first author (Wen Yi, yiwen@ustc.edu.cn). The data are not publicly available due to institutional restrictions. TIMED/SABER data are available at http://saber.gats-inc.com. The NAVGEM-HA data used in this study can be obtained from https://map.nrl.navy.mil/map/pub/nrl/navgem.

## Acknowledgements

This work was supported by the USTC Research Funds of the Double First-Class Initiative (YD3420002004), the National Natural Science Foundation of China (42125402, 41974174, 42188101, 41831071, 42174183, and 41904135), the B-type Strategic Priority Program of CAS (XDB41000000), the Project of Stable Support for Youth Team in Basic Research Field, CAS (YSBR-018), the Fundamental Research Funds for the Central Universities, the Anhui Provincial Natural Science Foundation (2008085MD113), and the Joint Open Fund of Mengcheng National Geophysical Observatory (MENGO-202209).

## Conflict of interest

The authors declare that they have no conflict of interest.

## Biographies

**Wen Yi** is an Associate Research Fellow at the School of Earth and Space Sciences (ESS), University of Science and Technology of China (USTC). He received his Ph.D. degree in Space Physics from USTC in 2018. He was awarded the Excellent Doctoral Dissertation of the Chinese Geophysical Society in 2019. His current research focuses on the solar-terrestrial influences on the mesosphere and lower thermosphere, and remote sensing of the mesosphere and lower thermosphere using atmosphere radars.

**Xianghui Xue** now serves as a Full Professor at the School of Earth and Space Sciences (ESS), University of Science and Technology of China (USTC). He received his Ph.D. degree from USTC in 2007. He joined the ESS of USTC after graduation. He was supported by the National Science Foundation for Distinguished Young Scholars in 2022. His research has been focusing on the middle and upper atmospheric dynamics and modeling, and atmospheric remote sensing based on the optical and radio technique.

## References

[1] Fritts D C, Alexander J M. Gravity wave dynamics and effects in the middle atmosphere. *Reviews of Geophysics,* **2003**, *41* (1): 1003.
[2] Frobes J M, Garrett H B. Theoretical studies of atmospheric tides. *Reviews of Geophysics and Space Physics,* **1979**, *17* (8): 1951–1981.
[3] Hocking W K, Fuller B, Vandepeer B. Real-time determination of meteor-related parameters utilizing modern digital technology. *Journal of Atmospheric and Solar-Terrestrial Physics,* **2001**, *63*: 155–169.
[4] Holdsworth D A, Reid I M, Cervera M A. Buckland Park all-sky interferometric meteor radar. *Radio Science,* **2004**, *39*: RS5009.
[5] Ma Z, Gong Y, Zhang S, et al. Study of mean wind variations and gravity wave forcing via a meteor radar chain and comparison with HWM-07 results. *Journal of Geophysical Research: Atmospheres,* **2018**, *123* (17): 9488–9501.
[6] Stober G, Kuchar A, Pokhotelov D, et al. Interhemispheric differences of mesosphere–lower thermosphere winds and tides investigated from three whole-atmosphere models and meteor radar observations. *Atmospheric Chemistry and Physics,* **2021**, *21* (18): 13855–13902.
[7] Zhou B Z, Xue X H, Yi W, et al. A comparison of MLT wind between meteor radar chain and SD-WACCM results. *Earth and Planetary Physics,* **2022**, *6* (5): 451–464.
[8] Yu Y, Wan W, Ning B, et al. Tidal wind mapping from observations of a meteor radar chain in December 2011. *Journal of Geophysical Research: Space Physics,* **2013**, *118* (5): 2321–2332.
[9] Stober G, Janches D, Matthias V, et al. Seasonal evolution of winds, atmospheric tides, and Reynolds stress components in the Southern Hemisphere mesosphere–lower thermosphere in 2019. *Annales Geophysicae,* **2021**, *39* (1): 1–29.
[10] Wang J C, Palo S E, Forbes J M, et al. Unusual quasi 10-day planetary wave activity and the ionospheric response during the 2019 Southern Hemisphere sudden stratospheric warming. *Journal of Geophysical Research: Space Physics,* **2021**, *126* (6): e2021JA029286.
[11] Wang J, Yi W, Chen T, et al. Quasi-6-day waves in the mesosphere and lower thermosphere region and their possible coupling with the QBO and solar 27-day rotation. *Earth and Planetary Physics,* **2020**, *4* (3): 285–295.
[12] Gu S Y, Lei J, Dou X, et al. The modulation of the quasi-two-day wave on total electron content as revealed by BeiDou GEO and meteor radar observations over central China. *Journal of Geophysical Research: Space Physics,* **2017**, *122* (10): 10651–10657.
[13] Holdsworth D A, Morris R J, Murphy D J, et al. Antarctic mesospheric temperature estimation using the Davis mesosphere-stratosphere-troposphere radar. *Journal of Geophysical Research: Atmospheres,* **2006**, *111*: D05108.
[14] Hocking W K, Singer W, Bremer J, et al. Meteor radar temperatures at multiple sites derived with SKiYMET radars and compared to OH, rocket and lidar measurements. *Journal of Atmospheric and Solar-Terrestrial Physics,* **2004**, *66*: 585–593.
[15] Hall C M, Aso T, Tsutsumi M, et al. Neutral air temperatures at 90 km and 70°N and 78°N. *Journal of Geophysical Research: Atmospheres,* **2006**, *111*: D14105.
[16] Yi W, Xue X, Chen J, et al. Estimation of mesopause temperatures at low latitudes using the Kunming meteor radar. *Radio Science,* **2016**, *51* (3): 130–141.
[17] Yi W, Xue X, Reid I M, et al. Climatology of interhemispheric mesopause temperatures using the high-latitude and middle-latitude meteor radars. *Journal of Geophysical Research: Atmospheres,* **2021**, *126* (6): e2020JD034301.
[18] Yi W, Xue X, Reid I M, et al. Estimation of mesospheric densities at low latitudes using the Kunming meteor radar together with SABER temperatures. *Journal of Geophysical Research: Space Physics,* **2018**, *123* (4): 3183–3195.
[19] Yi W, Xue X, Reid I M, et al. Climatology of the mesopause relative density using a global distribution of meteor radars. *Atmospheric Chemistry and Physics,* **2019**, *19* (11): 7567–7581.
[20] Rees D, Branett J J, Labitske K. COSPAR International Reference


DOI: 10.52396/JUSTC-2022-0158
*JUSTC*, **2023**, 53(5): 0501

Atmosphere: 1986, Part II, Middle Atmosphere Models. *Advances in Space Research,* **1990**, *10* (12): 357–517.
[21] Picone J M, Hedin A E, Drob D P, et al. NRLMSISE-00 empirical model of the atmosphere: Statistical comparisons and scientific issues. *Journal of Geophysical Research: Space Physics,* **2002**, *107* (A12): 1468.
[22] Drob D P, Emmert J T, Crowley G, et al. An empirical model of the Earth' s horizontal wind fields: HWM07. *Journal of Geophysical Research: Space Physics,* **2008**, *113*: A12204.
[23] Tang Q, Zhou Y, Du Z, et al. A comparison of meteor radar observation over China region with horizontal wind model (HWM14). *Atmosphere,* **2021**, *12* (1): 98.
[24] McCormack J, Hoppel K, Kuhl D, et al. Comparison of mesospheric winds from a high-altitude meteorological analysis system and meteor radar observations during the boreal winters of 2009–2010 and 2012–2013. *Journal of Atmospheric and Solar-Terrestrial Physics,* **2017**, *154*: 132–166.
[25] Stober G, Baumgarten K, McCormack J P, et al. Comparative study between ground-based observations and NAVGEM-HA analysis data in the mesosphere and lower thermosphere region. *Atmospheric Chemistry and Physics,* **2020**, *20* (20): 11979–12010.
[26] Jones J, Webster A R, Hocking W K. An improved interferometer design for use with meteor radars. *Radio Science,* **1998**, *33* (1): 55–65.
[27] Reid I M, McIntosh D L, Murphy, D J, et al. Mesospheric radar wind comparisons at high and middle southern latitudes. *Earth, Planets and Space,* **2018**, *70* (1): 84.
[28] Zeng J, Yi W, Xue X, et al. Comparison between the mesospheric winds observed by two collocated meteor radars at low latitudes. *Remote Sensing,* **2022**, *14* (10): 2354.
[29] Singer W, von Zahn U, Weiß J. Diurnal and annual variations of meteor rates at the arctic circle. *Atmospheric Chemistry and Physics,* **2004**, *4*: 1355–1363.
[30] Janches D, Palo S E, Lau E M, et al. Diurnal and seasonal variability of the meteoric flux at the South Pole measured with radars. *Geophysical Research Letters,* **2004**, *31*: L20807.
[31] Reid I M, Holdsworth D A, Morris R J, et al. Meteor observations using the Davis mesosphere-stratosphere-troposphere radar. *Journal of Geophysical Research: Space Physics,* **2006**, *111*: A05305.
[32] McCormack J P, Lynn Harvey V, Randall C E, et al. Intercomparison of middle atmospheric meteorological analyses for the Northern Hemisphere winter 2009–2010. *Atmospheric Chemistry and Physics,* **2021**, *21* (23): 17577–17605.
[33] Das S S, Kumar K K, Ramkumar G. First observations of quasi 120 day oscillation in mesospheric winds and temperature: Observations inferred from meteor radar. *Radio Science,* **2013**, *48*: 310–315.
[34] Yi W, Xue X, Chen J, et al. Quasi-90-day oscillation observed in the MLT region at low latitudes from the Kunming meteor radar and SABER. *Earth and Planetary Physics,* **2019**, *3* (2): 136–146.
[35] Guharay A, Batista P P, Buriti R A. Observations of a quasi-90-day oscillation in the MLT winds and tides over an equatorial station using meteor radar winds. *Advances in Space Research,* **2021**, *67* (10): 3125–3133.
[36] Gasperini F, Hagan M E, Zhao Y. Evidence of tropospheric 90 day oscillations in the thermosphere. *Geophysical Research Letters,* **2017**, *44* (20): 10125–10133.
[37] Reid I M, Spargo A J, Woithe J M. Seasonal variations of the nighttime O($^1$S) and O (8-3) airglow intensity at Adelaide, Australia. *Journal of Geophysical Research: Atmospheres,* **2014**, *119*: 6991–7013.
[38] Remsberg E, Damadeo R, Natarajan M, et al. Observed responses of mesospheric water vapor to solar cycle and dynamical forcings. *Journal of Geophysical Research: Atmospheres,* **2018**, *123* (7): 3830–3843.
[39] Luo J, Gong Y, Ma Z, et al. Long-term variation of lunar semidiurnal tides in the MLT region revealed by a meteor radar chain. *Journal of Geophysical Research: Space Physics,* **2022**, *127* (9): e2022JA030616.
[40] Li N, Luan X, Lei J, et al. Variations of mesospheric neutral winds and tides observed by a meteor radar chain over China during the 2013 sudden stratospheric warming. *Journal of Geophysical Research: Space Physics,* **2020**, *125* (5): e2019JA027443.
[41] Ma Z, Gong Y, Zhang S, et al. Understanding the excitation of quasi-6-day waves in both hemispheres during the September 2019 Antarctic SSW. *Journal of Geophysical Research: Atmospheres,* **2022**, *127* (3): e2021JD035984.
[42] Gu S Y, Li T, Dou X, et al. Long-term observations of the quasi two-day wave by Hawaii MF radar. *Journal of Geophysical Research: Space Physics,* **2013**, *118* (12): 7886–7894.
[43] Gu S Y, Li T, Dou X, et al. Observations of quasi-two-day wave by TIMED/SABER and TIMED/TIDI. *Journal of Geophysical Research: Atmospheres,* **2013**, *118* (4): 1624–1639.
[44] Gu S Y, Liu H L, Pedatella N M, et al. On the wave number 2 eastward propagating quasi 2 day wave at middle and high latitudes. *Journal of Geophysical Research: Space Physics,* **2017**, *122* (4): 4489–4499.
[45] Hindley N P, Mitchell N J, Cobbett N, et al. Radar observations of winds, waves and tides in the mesosphere and lower thermosphere over South Georgia island (54°S, 36°W) and comparison with WACCM simulations. *Atmospheric Chemistry and Physics,* **2022**, *22* (14): 9435–9459.


DOI: 10.52396/JUSTC-2022-0158
*JUSTC*, **2023**, 53(5): 0501